Journal of Physics: Conference Series **190** (2009) 012005 doi:10.1088/1742-6596/190/1/012005

Ab-initio CI calculations for 3*d* transition metal $L_{2,3}$ X-ray absorption spectra of $TiCl_4$ and $VOCl_3$

Hidekazu Ikeno[1], Frank M F de Groot[1] and Isao Tanaka[2,3]

[1] Department of Inorganic Chemistry and Catalysis, Utrecht University, Sorbonnelaan 16, 3584 CA Utrecht, The Netherlands

[2] Department of Materials Science and Engineering, Kyoto University, Yoshida, Sakyo, Kyoto 606-8501, Japan

[3] Nanostructures Research Laboratory, Japan Fine Ceramics Center, Atsuta, Nagoya 456-8587, Japan

E-mail: H.Ikeno@uu.nl

Abstract. X-ray-absorption near-edge structures (XANES) at the transition metal (TM) $L_{2,3}$-edge of $TiCl_4$ and $VOCl_3$ are calculated by the all-electron configuration interaction (CI) method using fully-relativistic molecular spinors with density functional theory (DFT). The electronic excitation from molecular spinors mainly composed of ligand p atomic spinors to those of TM-3d spinors, i.e., the charge transfer, is included by taking additional electronic configurations in the CI. The effects of the ligand field and the charge transfer on the TM-$L_{2,3}$ XANES are investigated by an *ab-intio* method. The reduction of inter-electron interaction due to the covalent bonding between TM and ligand atoms has been found. The contribution of charge transferred configuration is small at the initial state of TM-$L_{2,3}$ XANES while the significant amount of charge transferred configuration is found at the final states. The spectral shapes of TM-$L_{2,3}$ XANES of both $TiCl_4$ and $VOCl_3$ are strongly modified by the charge transfer effects.

1. Introduction

X-ray absorption spectroscopy (XAS) is a powerful technique for the characterization of materials and has been widely used in materials science[1; 2]. Fine structures that appear near the absorption edges (XANES) provide us with information about oxidation states, spin states, chemical bonding, and atomic coordinates[3; 4]. Recent developments of third generation synchrotron sources enable XANES measurement of very small concentrations with good energy resolution. In order to extract the information about the local environment of probe atoms, reliable theoretical tools which have predictive performance and that are free from adjustable parameters are indispensable. In this paper, we focus on the 3d transition metal (TM) $L_{2,3}$-edge XANES. At the edge, TM-2p core electrons are excited with the electric dipole transition into unoccupied 3d and 4s valence states. The transition matrix elements to the 4s states are negligible and the spectra are dominated by the 2p3d transitions. Because of the strong interactions among core TM-2p and 3d electrons, the shape of $L_{2,3}$ XANES is strongly modified from the empty 3d density of states: this is known as multiplet effects[5; 6]. In order to treat the electronic transition from core levels, relativistic effects should also be considered. In many 3d-TM compounds, neighboring ligand atoms contribute to the spectral shapes of $L_{2,3}$ XANES. The charge transfer from ligand ions to the TM ions plays an important role on the spectral

shapes of $L_{2,3}$ XANES of some $3d$ TM compounds. Thus, the contribution of ligand ions should be properly included in the calculation of TM-$L_{2,3}$ XANES. The most prevalent and conventional theoretical approach for the analysis of TM-$L_{2,3}$ XANES is the semi-empirical charge transfer multiplet method, where crystal field effects are incorporated into an atomic multiplet calculation using the group theoretical formalism[7]. In this approach, the ligand field effects are considered using the empirical parameters. Hence it has little predictive performance of the multiplet structures a priori. Recently, the Tanaka group in Kyoto has developed an *ab-intio* configuration interaction (CI) program for the x-ray absorption spectra. The molecular spinors obtained by relativistic density functional theory (DFT) are used as basis function for the CI calculations. All ligand field effects are included by using molecular spinors instead of atomic spinors. The spin-orbit coupling at the core $2p$ levels can be automatically taken into account by solving Dirac equation. The one-electron and the two-electron integrals, which determine the multiplet energies are directly evaluated over molecular spinors. Experimental spectra from many compounds having different d-electron numbers and coordination numbers have been successfully reproduced without any empirical parameters [8; 9; 10; 11]. The charge transfer from ligand to TM spinors can be included by taking additional electronic configuration in the CI[12]. In the present work, the *ab-intio* CI method is applied to the calculation for TM-$L_{2,3}$ XANES of $TiCl_4$ and $VOCl_3$ molecules. The electronic interactions among all electrons are rigorously calculated. The influences of the ligand field and the charge transfer from ligand to TM atoms on the multiplet structure and the spectral shapes are discussed.

2. Theoretical method

In this letter, TM-$L_{2,3}$ XANES of $TiCl_4$ and $VOCl_3$ molecules have been calculated by means of the *ab-intio* configuration interaction (CI) calculations. Details of our method have been described in Ref. [12]. In this section, we briefly recall the method.

An effective many-body Hamiltonian most commonly used for relativistic calculations for atoms and molecules is the 'no-pair' Hamiltonian[13; 14], which is described in the second quantized form as

$$\hat{H} = \sum_{i,j=1}^{L} \langle i|\hat{h}|j\rangle a_i^\dagger a_j + \frac{1}{2} \sum_{i,j,k,l=1}^{L} \langle ij|\hat{g}|kl\rangle a_i^\dagger a_j^\dagger a_l a_k, \tag{1}$$

where i, j, k and l indicate molecular spinors, N is the number of electrons in the system, and $L > N$ is the number of given molecular spinors. $a_i^\dagger$ and a_i denote the creation and the annihilation operators for an electron in the i'th spinor, respectively. $\langle i|\hat{h}|j\rangle$ and $\langle ij|\hat{g}|kl\rangle$ are the one-electron and the two-electron integrals over four-component molecular spinors. In the most general case, the numbers of independent one- and two-electron integrals are $L(L+1)/2$ and $(L(L+1)/2)^2$, respectively. $\hat{h}$ is the single-particle Dirac operator

$$\hat{h} = c\boldsymbol{\alpha} \cdot \boldsymbol{p} + mc^2\beta + v_{\text{ext}} \tag{2}$$

with v_{ext} the electrostatic potential from nuclei, and $\hat{g}$ in (1) is the Electron-electron interaction operator. The explicit form of $\hat{g}$ is given in Sec. 3.

The many-electron wavefunction is expressed as a linear combination of Slater determinants,

$$|\Psi_k\rangle = \sum_p C_{pk} |\Phi_p\rangle , \tag{3}$$

where $|\Phi_p\rangle = a_{p_1}^\dagger \cdots a_{p_N}^\dagger |\text{vac}\rangle$ is a Slater determinant constructed from $p_1, \ldots, p_N$-th molecular spinors, and $|\text{vac}\rangle$ denotes the vacuum state. The coefficients C_{pk} in (3) are determined by the

standard Rayleigh-Ritz variational method. The equation to be actually solved is the standard eigenvalue equation

$$\boldsymbol{H}\boldsymbol{C}_k = E_k \boldsymbol{C}_k, \tag{4}$$

$$H_{pq} = \sum_{i,j=1}^{L} \langle i|\hat{h}|j\rangle \langle \Phi_p|a_i^\dagger a_j|\Phi_q\rangle + \frac{1}{2}\sum_{i,j,k,l=1}^{L} \langle ij|\hat{g}|kl\rangle \langle \Phi_p|a_i^\dagger a_j^\dagger a_l a_k|\Phi_q\rangle. \tag{5}$$

The Hamiltonian matrix is fully diagonalized to obtain all possible initial and final states under the restricted electronic configurations. Then, the oscillator strength of the electric dipole transition is evaluated as

$$I_{if} = \frac{2m}{\hbar^2}(E_f - E_i)\left|\left\langle \Psi_f \left| \sum_{k=1}^{N} \boldsymbol{\epsilon}\cdot\boldsymbol{r}_k \right| \Psi_i \right\rangle\right|^2, \tag{6}$$

where Ψ_i and Ψ_f are many-electron wave functions for the initial and final states, while E_i and E_f are their energies. The absorption cross section were obtained by broadening the oscillator strengths using Lorentz functions and by multiplying with the constant $2\pi^2\hbar^2\alpha/m$. The full width at half maximum (FWHM) of Lorentz function was set to 0.5 eV over the whole energy region. In the case of $3d$ TM-$L_{2,3}$ XANES, the quadrupole transitions or the higher order transitions are some hundred times weaker than the dipole transitions and can be neglected.

This CI method is known to overestimate the absolute transition energy systematically. This can be ascribed to the truncation of Slater determinants. In other words, this is due to the lack of minor contribution of electronic correlations. In the present study, the transition energy was corrected by the taking the energy difference between single-electron spinors for the Slater's transition state as a reference[8].

3. Computational details

In the present work, we have calculated TM-$L_{2,3}$ XANES of $TiCl_4$ and $VOCl_3$ molecules. Atomic positions were obtained from the experimental data [15; 16]. A $TiCl_4$ molecule shows T_d symmetry with a Ti-Cl bond length of 2.170 Å, while a $VOCl_3$ molecule shows C_{3v} symmetry with V-Cl and V-O bond lengths are 2.142 Å and 1.570 Å, respectively. The relativistic single particle calculations were carried out by solving Dirac equations with the local density approximation (LDA) using `RSCAT` code[17]. In this code, four-component molecular spinors are described as linear combination of atomic spinors. The numerically generated four-component atomic spinors ($1s$–$4p$ for Ti and V, $1s$–$2p$ for O, and $1s$–$3p$ for Cl) were used as basis functions for molecular spinors.

Once molecular spinors were obtained, the one-electron integrals, $\langle i|\hat{h}|j\rangle$, and two-electron integrals, $\langle ij|\hat{g}|kl\rangle$ were directly evaluated over all possible combinations of molecular spinors by numerical integration. The many-electron Hamiltonian adopted in the present work is the 'no-pair' Dirac-Coulomb-Breit Hamiltonian, in which the inter-electron interaction operator $\hat{g}$ is described as

$$\hat{g} = \frac{1}{r_{ij}} + B(i,j). \tag{7}$$

The first term of $\hat{g}$ describes the instantaneous Coulomb interaction among electrons. The second term of $\hat{g}$ is the Breit interaction term, which is the first relativistic correction term for the inter-electron interaction in the quantum electrodynamics[18; 19]:

$$B(i,j) = -\frac{1}{2r_{ij}}\left\{\boldsymbol{\alpha}_i\cdot\boldsymbol{\alpha}_j + \frac{(\boldsymbol{\alpha}_i\cdot\boldsymbol{r}_{ij}\cdot\boldsymbol{\alpha}_i\cdot\boldsymbol{r}_{ij})}{r_{ij}^2}\right\}. \tag{8}$$

The Breit term contains the magnetic interaction introduced via the orbital and spin motions, and the retardation effect.

The influences of Breit interaction on the multiplet structures on the $3d$ TM-$L_{2,3}$ XANES have been systematically investigated in the previous work[20]. The main contribution of the Breit interactions is the reduction of the energy separation between L_3 and L_2 edges.

Because of the limitation of computational power, we restrict the number of Slater determinants expanding many-electron wave functions. The most preliminary condition for TM-$L_{2,3}$ XANES of $TiCl_4$ and $VOCl_3$ is just taking the electronic transition from $(\phi_{2p})^6(\phi_{3d})^0$ configuration to $(\phi_{2p})^5(\phi_{3d})^1$ configuration, where ϕ_{2p} and ϕ_{3d} denote the molecular spinors mainly composed of TM-$2p$ and $3d$ atomic spinors. Other core and valence spinors, i.e., molecular spinors mainly composed of TM $1s$, $2s$, $3s$, $3p$, Cl $1s$–$3p$ and O $1s$–$2p$ (only for $VOCl_3$) were assumed to be always occupied. The configurations having two or more holes on ϕ_{2p} were not considered, because the many-electron energies of such configurations are much higher and they do not significantly interact with these two configurations. Thus, the number of Slater determinants for initial state is ${}_6C_6 \times {}_{10}C_0 = 1$ while that for final states is ${}_6C_5 \times {}_{10}C_1 = 60$. Hereafter we refer this approach as the ligand field (LF) multiplet approach.

The charge transfer (CT) between ligand to TM atoms plays an important role on the spectral shapes of the TM-$L_{2,3}$ XANES of some $3d$ TM compounds. In the case of $TiCl_4$ and $VOCl_3$, the most important charge transfer channel is the electronic transition from ligand p (Cl-$3p$ and O-$2p$) to TM-$3d$ levels. In the *ab-intio* CI method based on the molecular spinors, a part of charge transfer through the covalent bonding between TM-$3d$ and ligand p levels are automatically included in the LF multiplet calculations by using molecular spinors instead of atomic ones. The other part of charge transfer effects can be included by taking the additional configurations (Slater determinants) in the CI. In order to investigate the latter contribution, we also performed charge transfer multiplet calculations by the *ab-intio* CI method. In this calculation, the charge transferred configuration $(\phi_{2p})^6(\phi_L)^{23}(\phi_{3d})^1$ and $(\phi_{2p})^5(\phi_L)^{23}(\phi_{3d})^2$ were added to describe the initial and the final states, respectively, where ϕ_L denotes the molecular spinors mainly composed of ligand p (Cl-$3p$ and O-$2p$) spinors. The inclusion of these configurations into CI significantly increases the number of Slater determinants and hence the dimension of the Hamiltonian matrix. The number of Slater determinants for initial and final states are ${}_6C_6 \times {}_{10}C_0 + {}_6C_6 \times {}_{24}C_{23} \times {}_{10}C_1 = 241$ and ${}_6C_5 \times {}_{10}C_0 + {}_6C_5 \times {}_{24}C_{23} \times {}_{10}C_2 = 6540$, respectively. The configurations with two or more excitation from ligand to TM-$3d$ were not considered because of the limitation of computational resources. Molecular spinors mainly composed of TM $1s$, $2s$, $3s$, $3p$, Cl $1s$–$3s$, O $1s$ and $2s$ (only for $VOCl_3$) were set to be fully occupied. We refer the latter approach as the LF+CT multiplet approach.

It should be noted that the relativistic spinors optimized for the initial states were used to construct the Slater determinants. Both the initial and the final states of TM-$L_{2,3}$ XANES were described using the same spinor set. The core-hole effects were not included in the spinors themselves, but they were included by taking the core-excited configurations into the CI calculations. It should also be noted that in our previous calculations for TM-$L_{2,3}$ XANES, the Slater determinants were constructed only from the particularly important molecular spinors, i.e., the spinors mainly composed of TM $2p$, $3d$ and ligand p atomic spinors. The electronic exchange and correlations among other electrons were approximately treated within the framework of DFT. In the present work, all spinors were considered explicitly to construct Slater determinants. In other words, all-electron CI calculations were performed.

4. Results and Discussions

At the first step of CI calculations for TM-$L_{2,3}$ XANES, we made relativistic density functional calculations for $TiCl_4$ and $VOCl_3$ molecules within LDA. The spin-orbit coupling in TM-$2p$ levels were automatically included by solving Dirac equation. In the $TiCl_4$ molecule with T_d

Table 1. Molecular spinor energy relative to the highest occupied spinor (ϵ), Mulliken population of ligand p atomic spinors ($Q_{\text{Cl-3p}}$ and $Q_{\text{O-2p}}$), and averaged values of the Coulomb integrals for the ϕ_{3d} molecular spinors. The values inside parentheses on the last column indicate the reduction factors of the Coulomb integrals from the corresponding atomic values.

	ϵ (eV)	$Q_{\text{Cl-3p}}$	$Q_{\text{O-2p}}$	$\langle ij\|r_{12}^{-1}\|ij\rangle_{\text{ave}}$ (eV)
$TiCl_4$				
e	4.34	0.157	—	15.03 (0.687)
t_2	5.21	0.192	—	14.12 (0.648)
$VOCl_4$				
$e(1)$	3.72	0.192	0.035	15.12 (0.611)
$e(2)$	4.99	0.130	0.166	14.89 (0.602)
a_1	5.94	0.109	0.203	14.27 (0.577)

symmetry, Ti-3d levels split into two levels, namely, e and t_2 because of the ligand field. In the $VOCl_3$ molecule, t_2 levels further split into e and a_1 levels due to the reduction of symmetry from T_d to C_{3v}. The eigenvalues of molecular spinors relative to the highest occupied spinor are shown in Table 1. Strictly speaking, t_2 levels with T_d symmetry further split because of the spin-orbit coupling at TM-3d levels. The expressions such as e and t_2 are not rigorously right within the relativistic theory. Instead, the representations of the double group, such as γ_7 and γ_8, should be employed. However, the relativistic effects on TM-3d levels are small and the familiar expression, e and t_2, is used for simplicity.

In the case of both $TiCl_4$ and $VOCl_3$, there is strong covalent bonding between TM-3d and ligand atomic spinors. The Mulliken population[21] of ligand p (Cl-3p and O-2p) atomic spinors is summarized in Table 1. One can find that the population of Cl-3p atomic spinors is 15.7% in e levels for $TiCl_4$. The Cl-3p population is greater in t_2 than e. In the case of $VOCl_3$, the Cl-3p (O-2p) populations decrease (increase) with increase of molecular spinor energies. The total contribution of ligand spinors becomes larger for $e(1)$, $e(2)$ and a_1, in that order.

The multiplet energies are obtained as eigenvalues of Hamiltonian matrix (5). Therefore, the multiplet energies depend on the one-electron integrals, $\langle i|\hat{h}|j\rangle$, and two-electron integrals, $\langle ij|\hat{g}|kl\rangle$. $\langle i|\hat{h}|j\rangle$ describes the ligand field splitting and the hopping integrals among molecular spinors, while $\langle ij|\hat{g}|kl\rangle$ denotes the inter-electron interaction energies. Since $\langle i|\hat{h}|j\rangle$ and $\langle ij|\hat{g}|kl\rangle$ are directly evaluated over molecular spinors, they are affected by the covalency and the crystal field effects.

In Table 1, the averaged value of Coulomb integrals in each molecular spinors is also shown. The values inside the parentheses indicate the reduction factors from Coulomb integrals among TM-3d atomic spinors. One can find that Coulomb integrals among ϕ_{3d} molecular spinors are significantly reduced from the atomic value. It should be noted that the reduction factors differ in each level. In the case of $TiCl_4$, for instance, the Coulomb integral among t_2 levels is more reduced than that among e levels. The reduction of Coulomb integrals becomes larger when the covalency between TM-3d and ligand p spinors is large.

We note that the reduction factors of Coulomb integrals among ϕ_{3d} levels for $TiCl_4$ are much smaller than those for $SrTiO_3$ which we have reported in the previous work[12], though Ti ions in $SrTiO_3$ and $TiCl_4$ are both 4+ ($3d^0$) at the ground state. The reduction factors for t_{2g} and e_g spinors are only 0.845 and 0.816, respectively. The reduction factor of the Coulomb integrals strongly depends on the covalency and the crystal fields.

The multiplet structures corresponding to TM-$L_{2,3}$ XANES of $TiCl_4$ and $VOCl_3$ have been

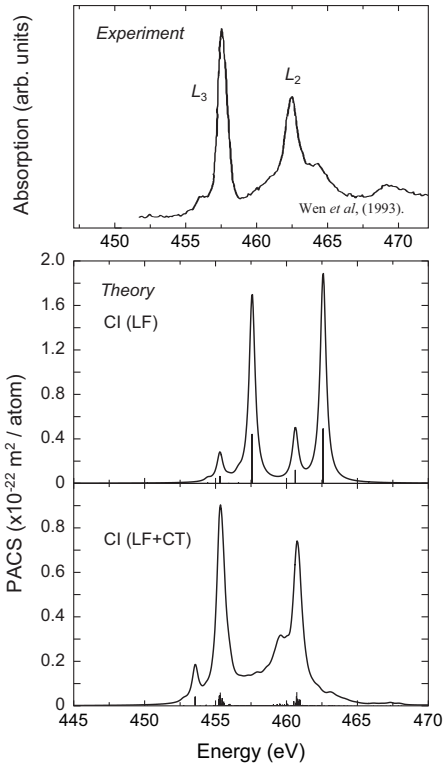

Figure 1. Theoretical Ti-$L_{2,3}$ XANES for $TiCl_4$ obtained by the LF multiplet approach (middle) and the LF+CT multiplet approach by the *ab-intio* CI method (bottom). They are compared with experimental spectrum taken from ref. [22]. Solid bars drawn with theoretical spectra are the oscillator strengths for the many-electron eigenstates.

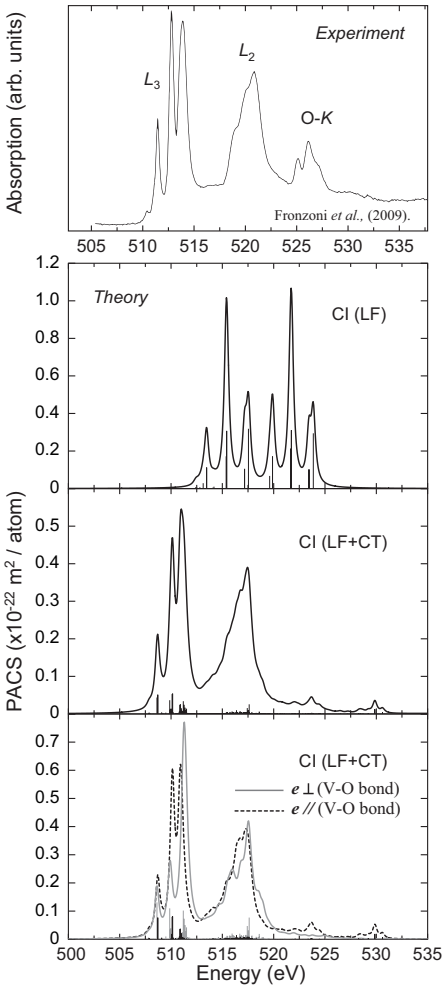

Figure 2. Theoretical V-$L_{2,3}$ XANES for $VOCl_3$ obtained by the LF multiplet approach (second upper) and the LF+CT multiplet approach by the *ab-intio* CI method (second lower). The orientation dependence of theoretical spectra is also shown (bottom). They are compared with experimental spectrum taken from ref. [23]. Solid bars drawn with theoretical spectra are the oscillator strengths for the many-electron eigenstates.

calculated by both the LF multiplet approach and the LF+CT multiplet approach. The many-electron Hamiltonian have been diagonalized in the space spanned by the restricted configurations as described in Sec. 3. The oscillator strengths of electric dipole transitions from the initial state to the all possible final states have been evaluated using (6). They were convolved with Lorentz functions to obtain photo-absorption cross section (PACS). The results are shown in figures 1 and 2. They are compared with the experimental spectra taken from literature[22; 23]. One can find large discrepancies between the theoretical spectrum calculated by the LF multiplet

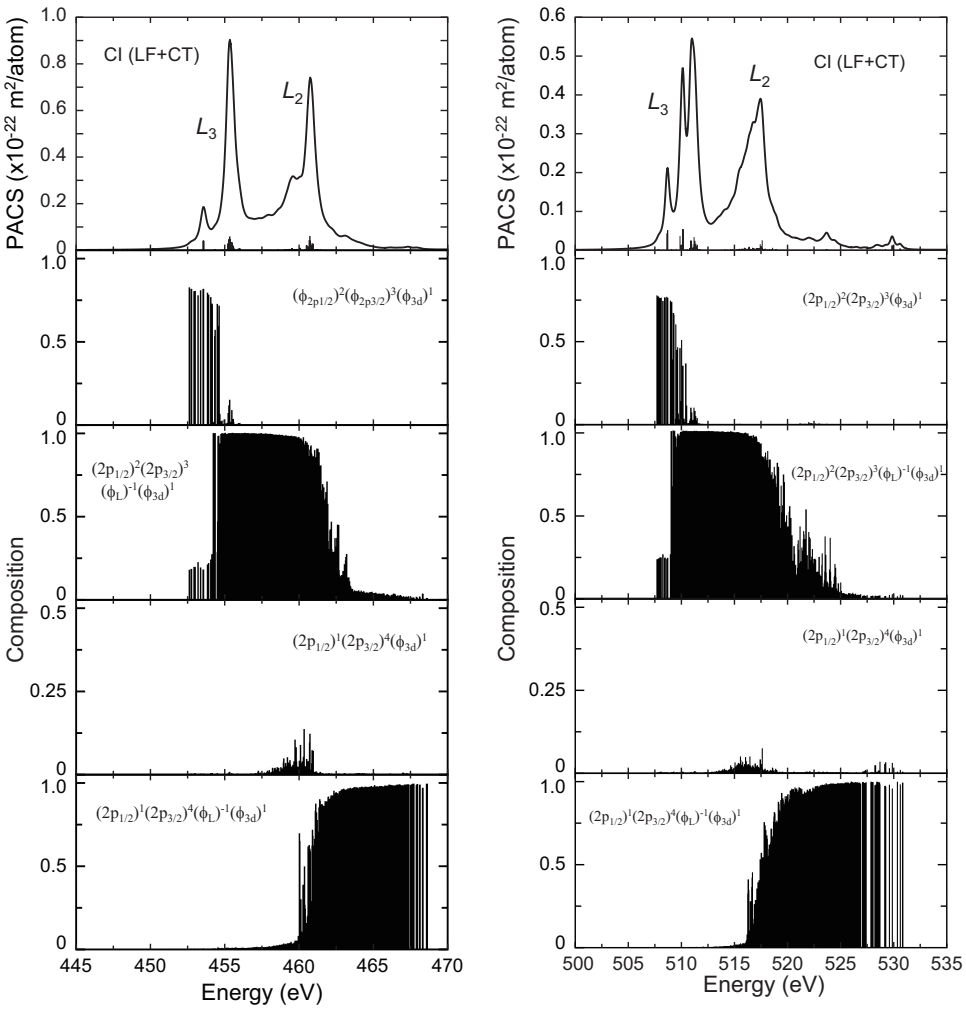

Figure 3. Theoretical Ti-$L_{2,3}$ XANES for $TiCl_4$ (left) and V-$L_{2,3}$ XANES for $VOCl_4$ (right) obtained by the LF+CT multiplet approach by *ab-intio* CI method. Lower panels show the composition of four different final configurations for many-electron eigenstates.

approach and the experimental spectrum for both $TiCl_4$ and $VOCl_3$ molecules. In the LF multiplet results, the L_3 and the L_2 spectra have similar shapes, while the L_3 and the L_2 shapes are markedly different in the experimental results. In addition, the relative peak positions are not reproduced by the LF multiplet approach. The main peaks appear in the L_3 region split further compared to the experimental results. The results show that further electronic correlations must be taken into account to interpret those spectra.

One can clearly see from Fig. 1 and 2 that, in both molecules, the spectral shapes drastically change when the charge transfer (CT) from ϕ_L to ϕ_{3d} levels is taken into account. The splitting between main peaks is much reduced by including the CT. Each peak in L_2 region is much broadened from that obtained in the LF multiplet approach. In addition, the CT creates widely spread satellite peaks above the L_2 main peaks. The theoretical spectra obtained by the LF+CT multiplet approach show much better agreement with the experimental ones than the LF multiplet results. The major features of TM-$L_{2,3}$ XANES are well reproduced in both $TiCl_4$ and $VOCl_3$.

In order to investigate the CT effects in detail, configuration analysis of many-electron

wavefunctions have been carried out. Considering the orthonormality of the Slater determinants, the composition of the p-th Slater determinant in the k-th eigenstate is simply given by $|C_{pk}|^2$. In both $TiCl_4$ and $VOCl_3$ molecules, the initial state obtained by the LF multiplet approach is completely composed of $(\phi_{3d})^0$ configuration. In the LF+CT multiplet approach, the initial state is still dominated by $(\phi_{3d})^0$ configuration, whose composition at initial state is 97.0% and 97.8% for $TiCl_4$ and $VOCl_3$, respectively. The contribution of charge transferred configuration $(\phi_L)^{-1}(\phi_{3d})^1$ is small at the initial state, where $(\phi_L)^{-1}$ indicates the hole on ϕ_L molecular spinors.

Figure 3 shows the compositions of four final electronic configurations, $(\phi_{2p_{3/2}})^{-1}(\phi_{3d})^1$, $(\phi_{2p_{1/2}})^{-1}(\phi_{3d})^1$, $(\phi_{2p_{3/2}})^{-1}(\phi_L)^{-1}(\phi_{3d})^2$, and $(\phi_{2p_{1/2}})^{-1}(\phi_L)^{-1}(\phi_{3d})^2$ at the final states of TM-$L_{2,3}$ XANES for $TiCl_4$ and $VOCl_3$. The number of final states for TM-$L_{2,3}$ XANES in the LF+CT multiplet approach is 6540 for both molecules. Almost semi-continuous multiplet levels can be found in Fig. 3. Since the initial state of TM-$L_{2,3}$ XANES is dominated by $(\phi_{3d})^0$ configuration, the electric dipole transition to $(\phi_{2p_{3/2}})^{-1}(\phi_{3d})^1$ and $(\phi_{2p_{1/2}})^{-1}(\phi_{3d})^1$ configurations contribute to the oscillator strengths. One can clearly see in Fig. 3 that these configuration strongly interacts with the charge transferred configurations, $(\phi_{2p_{3/2}})^{-1}(\phi_L)^{-1}(\phi_{3d})^2$, and $(\phi_{2p_{1/2}})^{-1}(\phi_L)^{-1}(\phi_{3d})^2$. In the case of $TiCl_4$, the eigenstates below 454 eV, which are responsible for the first main peak at L_3-edge and the small shoulder peaks located below are dominated by $(\phi_{2p_{3/2}})^{-1}(\phi_{3d})^1$ configuration. However, the $(\phi_{2p_{3/2}})^{-1}(\phi_L)^{-1}(\phi_{3d})^2$ configuration mixes with those eigenstates about 20%. The eigenstates which are responsible for the most significant peak at Ti L_3-edge (455–456 eV) are predominantly composed by $(\phi_{2p_{3/2}})^{-1}(\phi_L)^{-1}(\phi_{3d})^2$ configuration. The composition of $(\phi_{2p_{3/2}})^{-1}(\phi_{3d})^1$ configuration at those eigenstates is only up to 15%. Reflecting the small $(\phi_{2p_{3/2}})^{-1}(\phi_{3d})^1$ contribution, the oscillator strength at each eigenstate in this energy region becomes much smaller than that in the case of the LF multiplet approach. At the eigenstates responsible for the Ti-L_2 peaks, $(\phi_{2p_{1/2}})^{-1}(\phi_{3d})^1$ configuration strongly interact with $(\phi_{2p_{3/2}})^{-1}(\phi_L)^{-1}(\phi_{3d})^2$ and $(\phi_{2p_{1/2}})^{-1}(\phi_L)^{-1}(\phi_{3d})^2$ configurations. Though the contribution of $(\phi_{2p_{1/2}})^{-1}(\phi_{3d})^1$ configuration is minor in the L_2 region, the eigenstates which potentially contribute to oscillator strengths are distributed in wide energy range. That is the reason why the L_2 peaks are much broadened compared with those calculated by LF multiplet approach. The small but non-negligible contribution $(\phi_{2p_{1/2}})^{-1}(\phi_{3d})^1$ configuration at the final state above 461 eV contribute to the formation of satellite peaks. Similar trends can be observed in the case of $VOCl_3$ (see Fig. 3).

In the case of Ti-$L_{2,3}$ XANES for $TiCl_4$, the broad satellite peaks centered at around 464 eV and 469 eV have been observed in the experimental spectrum. Fronzoni *et al.* have investigated the Ti-$L_{2,3}$ XANES for $TiCl_4$ by the relativistic two-component zeroth-order regular approximation and the time-dependent DFT (relativistic ZORA TDDFT)[24]. They have claimed that these satellite peaks can be ascribed to the transition to the Rydberg states (essentially, $4s$, $4p$ and $4d$). The main features as well as the satellite peaks of Ti-$L_{2,3}$ XANES were well reproduced by taking the basis set augmented with diffused functions for Ti atom. The relativistic ZORA TDDFT method has also been applied to the TM-$L_{2,3}$ XANES for $VOCl_3$ and other molecules[23; 25]. In the present work, we found that the satellite peaks just above the Ti-L_2 main peak of $TiCl_4$ were created by including the charge transfer from ϕ_L to ϕ_{3d} levels, though their intensities are smaller than those observed in the experimental spectrum. It is very interesting that the satellites can be explained either by the charge transfer $((\phi_{2p})^{-1}(\phi_{3d})^1+(\phi_{2p})^{-1}(\phi_{3d})^2(\phi_L)^{-1})$ or by the Rydberg states, for example $((\phi_{2p})^{-1}(\phi_{3d})^1+(\phi_{2p})^{-1}(\phi_{3d})^0(\phi_{4d})^1)$. The satellites can be related to $3d^2$ (CT) or $3d^0$ (Rydberg) final states, respectively. Further analysis for the assignment of these satellite peaks should be performed in the future.

5. Conclusions

All electron relativistic configuration interaction (CI) calculations were performed for TM-$L_{2,3}$ XANES of $TiCl_4$ and $VOCl_3$ molecules. All ligand field effects including the crystal field and the covalent bonding between TM and ligand atoms were automatically included by using molecular spinors. The Coulomb integrals among ϕ_{3d} molecular spinors were significantly reduced from the corresponding atomic values because of the strong covalent bonding between TM-3d and ligand p (Cl-3p and O-2p) atomic spinors. The reduction factor of the Coulomb integrals strongly depends on the covalency and the crystal field.

The charge transfer from ϕ_L to ϕ_{3d} levels was included in the CI by adding $(\phi_L)^{-1}(\phi_{3d})^1$ and $(\phi_{2p})^{-1}(\phi_L)^{-1}(\phi_{3d})^2$ configurations for the initial and the final states, respectively. The main features of experimental spectra were well reproduced by including the charge transfer effects. At the initial state of TM-$L_{2,3}$ XANES, the contribution of $(\phi_L)^{-1}(\phi_{3d})^1$ configuration is small. In contrast, strong configuration interaction between $(\phi_{2p})^{-1}(\phi_{3d})^1$ and $(\phi_{2p})^{-1}(\phi_L)^{-1}(\phi_{3d})^2$ configurations was observed at the final states of TM-$L_{2,3}$ XANES for $TiCl_4$ and $VOCl_3$ molecules. In the L_2 region, the final states with small composition of $(\phi_{2p_{1/2}})^{-1}(\phi_{3d})^1$ configuration, which is dipole allowed configuration from $(\phi_{3d})^0$ configuration, are formulated in the wide energy range. This results in the broadening of the L_2 main peaks and the formation of widely spread satellite peaks.

Acknowledgments

H.I. and F.d.G. acknowledge financial support from the Netherlands National Science Foundation (NWO/VICI program).

References

[1] Koningsberger D C and Prins R (eds) 1988 *X-Ray Absorption: Principles, Applications, Techniques of EXAFS, SEXAFS and XANES* Chemical Analysis: A Series of Monographs on Analytical Chemistry and Its Applications (New York: John Wiley & Sons, Inc.)

[2] Kawai J 2000 *Encyclopedia of Analytical Chemistry* (Chichester: John Wiley & Sons, Inc.) chap Absorption Techniques in X-ray Spectrometry, pp 13288–13315

[3] Stöhr J 1992 *NEXAFS Spectroscopy* Springer Series in Surface Sciences (Berlin: Springer Verlag)

[4] Chen J G 1997 *Surf. Sci. Rep.* **30** 1–152

[5] de Groot F M F, Fuggle J C, Thole B T and Sawatzky G A 1990 *Phys. Rev. B* **41** 928–937

[6] de Groot F M F, Fuggle J C, Thole B T and Sawatzky G A 1990 *Phys. Rev. B* **42** 5459–5468

[7] de Groot F and Kotani A 2008 *Core Level Spectroscopy of Solids* Advances in Condensed Matter Science (CRC Press)

[8] Ogasawara K, Iwata T, Koyama Y, Ishii T, Tanaka I and Adachi H 2001 *Phys. Rev. B* **64** 115413

[9] Ikeno H, Mizoguchi T, Koyama Y, Kumagai Y and Tanaka I 2006 *Ultramicroscopy* **106** 970–975

[10] Ikeno H, Tanaka I, Koyama Y, Mizoguchi T and Ogasawara K 2005 *Phys. Rev. B* **72** 075123

[11] Kumagai Y, Ikeno H, Oba F, Matsunaga K and Tanaka I 2008 *Phys. Rev. B* **77** 155124

[12] Ikeno H, de Groot F M F, Stavitski E and Tanaka I 2009 *J. Phys.: Condens. Matter* **21** 104208

[13] Sucher J 1980 *Phys. Rev. A* **22** 348–362

[14] Mittleman M H 1981 *Phys. Rev. A* **24** 1167–1175

[15] Morino Y and Uehara H 1966 *J. Chem. Phys.* **45** 4543–4550

[16] Karakida K i and Kuchitsu K 1975 *Inorg. Chim. Acta* **13** 113–119
[17] Rósen A, Ellis D E, Adachi H and Averill F W 1976 *J. Chem. Phys.* **65** 3629–3634
[18] Breit G 1929 *Phys. Rev.* **34** 375–375
[19] Breit G 1932 *Phys. Rev.* **39** 616–624
[20] Ikeno H and Tanaka I 2008 *Phys. Rev. B* **77** 075127
[21] Mulliken R S 1955 *J. Chem. Phys.* **23** 1833–1840
[22] Wen A T and Hitchcock A P 1993 *Can. J. Chem.* **71** 1632–1644
[23] Fronzoni G, Stener M, Decleva P, de Simone M, Coreno M, Franceschi P, Furlani C and Prince K C 2009 *J. Phys. Chem. A* **113** 2914–2925
[24] Fronzoni G, Stener M, Decleva P, Wang F, Ziegler T, van Lenthe E and Baerends E J 2005 *Chem. Phys. Lett.* **416** 56–63
[25] Casarin M, Finetti P, Vittadini A, Wang F and Ziegler T 2007 *J. Phys. Chem. A* **111** 5270–5279